IEEE Access
Multidisciplinary | Rapid Review | Open Access Journal

Received 30 May 2022, accepted 23 June 2022, date of publication 29 June 2022, date of current version 8 July 2022.

Digital Object Identifier 10.1109/ACCESS.2022.3186996

RESEARCH ARTICLE

Fly-Around Control of Space Tumbling Target Under Multiple Constraints

SHUANG LIANG, YASHENG ZHANG, WEILIN WANG, AND LU JIA
Space Engineering University, Beijing 101416, China
Corresponding author: Shuang Liang (shuangshuangsmart@163.com)

ABSTRACT Aiming at the practical problems of external unknown disturbance and internal modeling uncertainty, when space tumbling target flies around in close range, a sliding mode controller (SMC) based on active disturbance rejection control (ADRC) technology is proposed to realize real-time estimation and compensation of ''total disturbance.'' Firstly, according to the motion characteristics of space tumbling target, the relative motion equation in rotating line of sight (RLOS) coordinate system is established; Secondly, the compound controller is designed, and the convergence of the nonlinear state expansion observer and the stability of the closed-loop system are analyzed based on the root locus method and Lyapunov function method respectively; Finally, the simulation results show that the SMC based on ADRC technology can effectively suppress the disturbance and overcome the chattering problem of traditional sliding mode controller. It has a good control quality, and strong robustness is an easy method for engineering practice.

INDEX TERMS RLOS, active disturbance rejection, uncertainty, stability, robustness.

I. INTRODUCTION

In 1957, when the Soviet Union successfully launched the first man-made satellite, human beings began to explore the mysteries of space. However, the continuous frequency and deepening of space activities have also brought a large amount of space debris such as rocket ejectors, failed satellites, discards, and collision fragments to the space environment. As of November 4, 2021, according to the USA space surveillance network, there are 23522 space targets, including 7824 spacecraft and 15698 rocket bodies and debris [1]. Much space debris has become the main pollution source of the space environment and poses a great threat to the development and safety of the aerospace industry. Therefore, the development of on-orbit repair, fuel filling, capture and recovery, and other on-orbit services is of great significance for promoting the on-orbit service capability and maintaining the safety and stability of the space environment [2]–[9].

Space debris often presents rolling motion states, such as spin and nutation, without cooperative identification, and some uncertain factors, such as orbital maneuvers, exist. It is difficult to accurately model the relative motion of such space tumbling targets [10], [11]. The space environment is complex, and spacecraft will be disturbed by the outside world, such as gravity gradient and solar light pressure, especially in short-range relative motion, which puts forward higher requirements for the accuracy, robustness, and stability of the control technology.

When studying relative motion control with non-cooperative targets, most of them follow the existing relative motion modeling methods of rendezvous, docking, and formation flights, which are mainly based on the local-vertical local-horizontal (LVLH) coordinate system and the line-of-sight (LOS) coordinate system. In addition, for non-cooperative targets, a few scholars have proposed a relative motion modeling method to improve the LOS coordinate system, such as the RLOS coordinate system and an integrated modeling method based on the dual quaternion [12]–[16].

A. RELATIVE MOTION CONTROL BASED ON THE LVLH COORDINATE SYSTEM

This method mainly includes the CW equation for a circular orbit proposed by Clohessy and Wiltshire [17] and the TH equation for an elliptical orbit further derived by Tschauner and Hempel [18]. The CW equation is a linearized equation to

The associate editor coordinating the review of this manuscript and approving it for publication was Halil Ersin Soken.

solve the relative motion of a spacecraft over a short distance; its precondition is that the target moves in a circular orbit, and the relative distance between two spacecraft is far less than the target's center distance. The TH equation is further derived to obtain analytical solutions related to the eccentricity and true near-point angle. The origin of the base coordinate system for the above two methods is established on the target spacecraft.

In [19], considering the motion characteristics of the space tumbling target, it is possible that the centroid and sensor do not coincide, the CW equation was modified, and a nonlinear suboptimal tracking controller was designed. In [20], an attitude orbit coupling equation was established based on the CW equation. The θ-D optimal control method was proposed to realize attitude orbit synchronization control of a large-angle maneuver. In [21], the TH equation was used to describe the autonomous rendezvous and approach mission of noncooperative targets in an elliptical orbit. The guidance error of tracking spacecraft caused by the dynamic characteristics of noncooperative targets was analyzed, and a guidance scheme based on a convex optimization algorithm was proposed. In [22], while studying the problem of short-range relative motion control, a robust adaptive controller was designed based on the CW equation. In [23], based on the CW equation, a terminal sliding mode adaptive controller considering disturbance was designed for the short-range rendezvous section of the space tumbling target. In [24] and [25], according to the analytical solution of the CW equation, a variety of fly around forms were proposed, and a sliding mode variable structure controller was designed to realize the six-degrees-of-freedom attitude orbit coupling control of spacecraft fly-around quickly. In [26], fast fly-around control was realized for noncooperative targets based on the CW equation. In [27], the fly-around and acquisition of a runaway rolling satellite were studied, with emphasis on the collision avoidance problem when the tracker flies over the target. In [28] and [29], the attitude orbit coupling model was established based on the TH equation and the error quaternion, and an adaptive method was designed to realize uncontrolled tumbling target tracking and approximation control to overcome external interference and system uncertainty.

In addition, many scholars have studied relative motion equations involving perturbations. In [30], a geometric method was proposed to study the relative motion using orbital element differences. This method can be easily used to study perturbation effects. In [31], the state transition matrix of relative motion was obtained using a geometric method that includes the influences caused by the eccentricity of the reference orbit, differential gravitational perturbations, and the equatorial bulge term J2. In [32] and [33], the CW equation was modified by Carter and Humi to include perturbations, and the dynamic equation of the relative motion in a central force field with linear drag was studied. In [34], a generalized analytical solution of relative motion dynamics with arbitrary perturbations was developed using orbital element difference.

B. RELATIVE MOTION CONTROL BASED ON THE LOS COORDINATE SYSTEM

In the relative motion control of noncooperative targets, a method based on the LOS coordinate system is widely used and has the most application prospects.

In [35], under the conditions of parameter uncertainty and external interference, a six-degrees-of-freedom relative motion equation was established based on the LOS coordinate system, and an adaptive finite-time tracking controller was designed to realize a noncooperative target fly-around control task. In [36], for a noncooperative target with maneuvering, a relative orbit dynamics equation based on the LOS coordinate system was established, and the θ-D method was designed for target tracking and approach control. In [37], aiming at the problem of forced fly-around noncooperative targets, a six-degrees-of-freedom attitude orbit coupling model considering control input and dynamic coupling factors was established based on the LOS coordinate system, and an adaptive control satisfying closed-loop stability under multiple constraints was designed. In [38], in the case of external interference, unmodeled dynamics, and thrust saturation, an adaptive control law was proposed to realize relative position tracking control of noncooperative targets in the LOS coordinate system. In [39], the Lyapunov method was designed to realize noncooperative target-tracking control based on the LOS coordinate system. In [40], the surveillance fly-around of noncooperative targets was realized based on the LOS coordinate system. In [41], the problem of obstacle avoidance guidance for autonomous rendezvous and docking with noncooperative spacecraft was studied based on the LOS coordinate system.

C. RELATIVE MOTION CONTROL BASED ON THE RLOS COORDINATE SYSTEM

The above relative motion modeling methods have the problem of insufficient representation of the motion state for space tumbling targets. Differential geometry is an effective method for studying the motion law of space curves. The curvature and torsion were used to describe the rotation of the space curve. It was initially used to deduce the space pure proportional guidance law (PPN) in the guidance field. Based on the differential geometry theory, Chiou *et al.* [42] first constructed the relative motion equation of projectiles under ideal conditions in the arc-length domain. Meng *et al.* [43] further derived the relative motion equation when the approaching velocity changed against the background of the rendezvous task. However, these methods are still based on an inertial coordinate system. Li *et al.* [44], [45] further studied the time-domain method, proposing the concepts of the RLOS coordinate system and instantaneous rotation plane of LOS (IRPL), and reduced the relative motion of curves in three-dimensional space to that in two-dimensional space based on the Frenet-Serret active frame theory. On this basis, in [46]–[50], a new relative motion modeling method was proposed to solve the practical problems of the relative

motion control of space-tumbling targets in the RLOS coordinate system. Augmented proportional navigation (APN), SMC, and so on were designed for this model.

At present, research on the control of the relative motion equation of space tumbling targets based on the RLOS coordinate system is still in its infancy, and there are few research results, especially on the control accuracy and robustness under multiple constraints, such as external interference, parameter uncertainty, unmodeled dynamic characteristics, and control input saturation.

In this study, the space tumbling target is considered as the research object, and the constraints of external disturbance and internal modeling uncertainty are considered to study the control problem of its close fly-around. In the closed fly-around stage, the tracker continuously measures the relative motion parameters with the space tumbling target by installing a microwave or optical sensor and guides the tracker to complete the fly-around mission. The thruster used in this study mainly adopts the PRISMA layout. There are six main thrusters, two in each group, which are placed in three directions, passing through the centroid of the tracker and perpendicular to each other. Among them, two groups are placed on the plane parallel to the solar panel to provide thrust in the Los direction, and the other group is placed in the direction perpendicular to the solar panel to provide thrust perpendicular to the LOS [48]. First, the relative motion equation in the RLOS coordinate system is derived and transformed into a form that is convenient for the controller design. Second, under the constraints of external disturbance and internal modeling uncertainty, the compound controller is designed based on two control methods: ADRC [51]–[56] and SMC [57]–[62]. The simulation results show that the controller designed in this study can effectively suppress the disturbance, overcome the chattering problem of the traditional SMC, and have good control quality and strong robustness.

II. RELATIVE MOTION MODEL

In this paper, the relative motion dynamic equation will be derived based on the RLOS coordinate system. First, the J2000 geocentric inertial coordinate system O_e-$X_eY_eZ_e$ is defined, as shown in Fig. 1. Geocentric O_e is the coordinate origin, the epoch equatorial plane is taken as the datum plane, O_eZ_e is the normal vector direction of the datum plane, the direction of O_eX_e axis points from geocentric to J2000 spring equinox, and O_eY_e is determined by the right-hand rule. The second is the LOS coordinate system O_s-$X_sY_sZ_s$, the coordinate origin O_s is located at the centroid of the tracker, the O_sY_s axis is the LOS direction pointing to the target centroid, the O_sZ_s axis is perpendicular to the O_sY_s axis in the vertical plane, the O_sX_s axis forms a right-hand system with the O_sY_s axis and O_sZ_s axis. The third is the RLOS coordinate system O_s-$e_re_\theta e_\omega$, the coordinate origin O_s is located at the centroid of the tracking spacecraft, $\boldsymbol{e}_r$ is the unit vector in the LOS direction, $\boldsymbol{e}_\omega$ is the unit vector in the LOS angular velocity direction, and $\boldsymbol{e}_\theta$ meets the right-hand coordinate system. $\boldsymbol{r}$ is

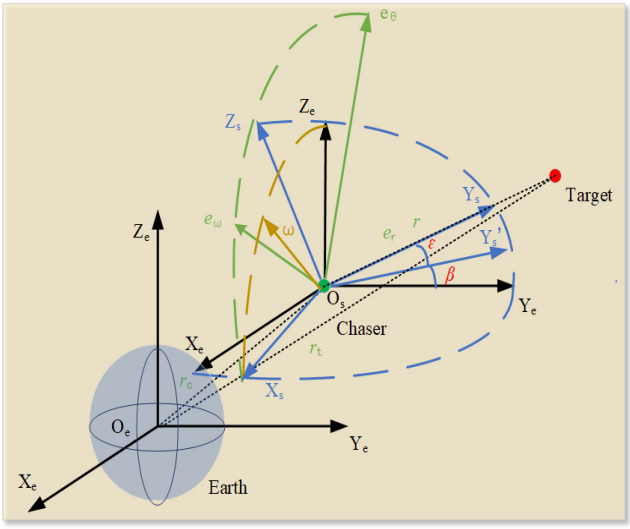

FIGURE 1. Relative motion coordinate system.

the relative position vector between the tracker and the target, ε is the altitude angle, β is the azimuth, $\boldsymbol{r}_c$ is the position vector of the tracker in J2000, and $\boldsymbol{r}_t$ is the position vector of the target in J2000.

The three-dimensional motion equation [44] established in the RLOS coordinate system is

$$\begin{cases} \dot{\boldsymbol{e}}_\mathrm{r} = \omega_\mathrm{s}\boldsymbol{e}_\theta \\ \dot{\boldsymbol{e}}_\theta = -\omega_\mathrm{s}\boldsymbol{e}_\mathrm{r} + \Omega_\mathrm{s}\boldsymbol{e}_\omega \\ \dot{\boldsymbol{e}}_\omega = -\Omega_\mathrm{s}\boldsymbol{e}_\theta \end{cases} \tag{1}$$

where $\boldsymbol{e}_\mathrm{r}$ and $\boldsymbol{e}_\theta$ constitute the IRPL; $\boldsymbol{e}_\omega$ is the normal vector of IRPL; $\Omega_\mathrm{s} \in \mathbb{R}$ is the angular velocity of rotation of $\boldsymbol{e}_\omega$ (IRPL around $\boldsymbol{e}_\mathrm{r}$), $\boldsymbol{\Omega}_\mathrm{s} = \Omega_\mathrm{s}\boldsymbol{e}_\mathrm{r}$; $\omega_s \in \mathbb{R}$ is the LOS rotation rate, $\boldsymbol{\omega}_\mathrm{s} = \omega_\mathrm{s}\boldsymbol{e}_\omega$.

The relative position vector between the tracker and the target is as follows:

$$\boldsymbol{r} = \boldsymbol{r}_\mathrm{t} - \boldsymbol{r}_\mathrm{c} \tag{2}$$

The LOS direction unit vector $\boldsymbol{e}_\mathrm{r}$ is as follows:

$$\boldsymbol{e}_r = \frac{\boldsymbol{r}}{r} \tag{3}$$

where $r \in \mathbb{R}$ is the relative distance between the tracker and the target.

After deriving Eq. (2) and Eq. (3), the relative velocity vector between the tracker and the target is as follows:

$$\boldsymbol{v} = \boldsymbol{v}_\mathrm{t} - \boldsymbol{v}_\mathrm{c} = \dot{r}\boldsymbol{e}_r + r\dot{\boldsymbol{e}}_r \tag{4}$$

The relative acceleration between the tracker and the target is derived from Eq. (4), and is expressed as follows:

$$\boldsymbol{a} = \dot{\boldsymbol{v}} = \ddot{r}\boldsymbol{e}_r + 2\dot{r}\dot{\boldsymbol{e}}_r + r\ddot{\boldsymbol{e}}_r \tag{5}$$

Substituting Eq. (1) into Eq. (5), the expression for relative acceleration is converted into Eq. (6).

$$\boldsymbol{a} = \ddot{r}\boldsymbol{e}_r + 2\dot{r}\omega_s\boldsymbol{e}_\theta + r(\dot{\omega}_s\boldsymbol{e}_\theta + \omega_s\dot{\boldsymbol{e}}_\theta)$$

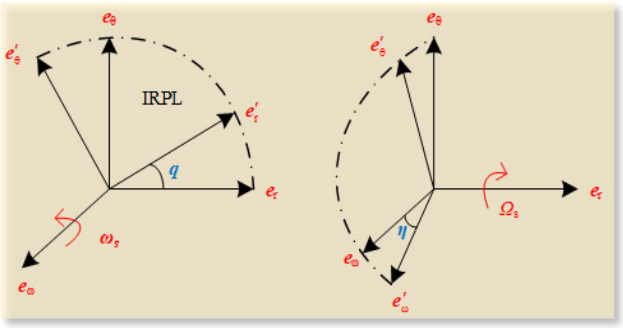

FIGURE 2. The LOS angle q and the IRPL angle η.

$$
\begin{aligned}
&= \ddot{r}\boldsymbol{e}_r + 2\dot{r}\omega_s\boldsymbol{e}_\theta + r\dot{\omega}_s\boldsymbol{e}_\theta + r\omega_s(-\omega_s\boldsymbol{e}_r + \Omega_s\boldsymbol{e}_\omega) \\
&= (\ddot{r} - r\omega_s^2)\boldsymbol{e}_r + (r\dot{\omega}_s + 2\dot{r}\omega_s)\boldsymbol{e}_\theta + r\omega_s\Omega_s\boldsymbol{e}_\omega \qquad (6)
\end{aligned}
$$

Eq. (6) can be rewritten into the following three sub- equations.

$$
\begin{cases}
\ddot{r} - r\omega_{\mathrm{s}}^2 = a_{\mathrm{tr}} - a_{\mathrm{cr}} \\
r\dot{\omega}_{\mathrm{s}} + 2\dot{r}\omega_{\mathrm{s}} = a_{\mathrm{t}\theta} - a_{\mathrm{c}\theta} \\
r\omega_{\mathrm{s}}\Omega_{\mathrm{s}} = a_{\mathrm{t}\omega} - a_{\mathrm{c}\omega}
\end{cases} \qquad (7)
$$

Among them, a_{t} and a_{c} are the control acceleration of the target and the tracker respectively, and the subscripts "r, θ, and ω" are the components of the control acceleration in the three directions of the RLOS coordinate system $\boldsymbol{e}_{\mathrm{r}}$, $\boldsymbol{e}_\theta$, and $\boldsymbol{e}_\omega$ respectively; The first two sub-equations determine the change law of r, $\dot{r}$, and ω_{s} in IRPL, and the third sub- equation determines the change law of Ω_{s}, when r and ω_{s} are constant.

As shown in Fig. 2, in the IRPL, the rotation angle of the LOS is defined as the LOS angle q, and the rotation angle of the normal vector of the IRPL is defined as the IRPL angle η. Two abstract variables in the equation of relative motion, the LOS rotation rate ω_{s} and IRPL rotation angular velocity Ω_{s}, are equivalently transformed and can be written as follows:

$$
\omega_{\mathrm{s}} = \dot{q} \quad \Omega_{\mathrm{s}} = \dot{\eta} \qquad (8)
$$

Considering the noncooperative characteristics of the space tumbling target, problems such as whether there is a maneuver in the motion state are attributed to the uncertainty of internal modeling, which are recorded as $F_{\mathrm{r}}(t)$, $F_\theta(t)$, and $F_\omega(t)$ in the direction of each coordinate axis, and the gravity gradient and solar light pressure are attributed to external disturbances, which are recorded as $w_{\mathrm{r}}(t)$, $w_\theta(t)$, and $w_\omega(t)$ in the direction of each coordinate axis. The uncertainty of the internal modeling and external disturbance is collectively referred to as the "total disturbance" of the system. Therefore, the relative motion equation can be rewritten as

$$
\begin{cases}
\ddot{r} - r\dot{q}^2 = F_{\mathrm{r}}(t) + w_{\mathrm{r}}(t) - a_{\mathrm{cr}} \\
r\ddot{q} + 2\dot{r}\dot{q} = F_\theta(t) + w_\theta(t) - a_{\mathrm{c}\theta} \\
r\dot{q}\dot{\eta} = F_\omega(t) + w_\omega(t) - a_{\mathrm{c}\omega}
\end{cases} \qquad (9)
$$

This study considers that in the actual fly-around process, the target orbit maneuvers (Ω_{s} is a constant value finally) or does not maneuver ($\Omega_{\mathrm{s}} = 0$), and the flying around in the above two cases can be realized in the IRPL without applying the control of the $\boldsymbol{e}_\omega$ direction [47]–[49]. To facilitate the design of the controller in the next step, the system object model should be transformed into a form of direct feedback, and new variables, $\boldsymbol{x}_1 = [r, q]^T \in \mathbb{R}^2$ and $\boldsymbol{x}_2 = [\dot{r}, \dot{q}]^T \in \mathbb{R}^2$, are defined. According to the new variables, $\boldsymbol{x}_1$ and $\boldsymbol{x}_2$, the relative motion equation can be rewritten as follows:

$$
\begin{cases}
\dot{\boldsymbol{x}}_1 = \boldsymbol{x}_2 \\
\dot{\boldsymbol{x}}_2 = f(\boldsymbol{x}_1, \boldsymbol{x}_2) + \boldsymbol{B}(\boldsymbol{F}(t) + \boldsymbol{w}(t) + \boldsymbol{u}) \\
\boldsymbol{y} = \boldsymbol{x}_1
\end{cases} \qquad (10)
$$

where

$$
\begin{aligned}
f(\boldsymbol{x}_1, \boldsymbol{x}_2) &= \begin{bmatrix} r\dot{q}^2 \\ -\dfrac{2\dot{r}\dot{q}}{r} \end{bmatrix} \in \mathbb{R}^2, \quad \boldsymbol{B} = \begin{bmatrix} 1 & 0 \\ 0 & \dfrac{1}{r} \end{bmatrix} \in \mathbb{R}^{2\times 2}, \\
\boldsymbol{F}(t) &= [\boldsymbol{F}_{\mathrm{r}}(t), \boldsymbol{F}_\theta(t)]^T \in \mathbb{R}^2, \\
\boldsymbol{w}(t) &= [\boldsymbol{w}_{\mathrm{r}}(t), \boldsymbol{w}_\theta(t)]^T \in \mathbb{R}^2, \\
\boldsymbol{u} &= [-a_{\mathrm{cr}}, -a_{\mathrm{c}\theta}]^T \in \mathbb{R}^2.
\end{aligned}
$$

III. CONTROL PROBLEM DESCRIPTION

During the actual on-orbit operation and fly-around, there are the following practical problems: space debris often presents spin, nutation, and other motion states, without a cooperative logo, and some uncertain factors such as orbital maneuvers exist that make it difficult to accurately model the relative motion of such space tumbling targets, which are disturbed by gravity gradient, solar light pressure, and other external disturbances during on-orbit operation, which are also difficult to determine. To further design the controller and facilitate simulation verification, the following reasonable assumptions are made:

Assumption 1: The tumbling target is a regular precession target whose precession angle (ψ) rate and spin angle (φ) rate are constant; the nutation angle (θ) rate is 0.

Assumption 2: External disturbances $w_r(t)$ and $w_\theta(t)$ are unknown and bounded, and the boundary is an unknown constant.

Assumption 3: The internal unmodelled dynamics of $F_r(t)$ and $F_\theta(t)$ are unknown and bounded, and the boundary is an unknown constant.

Control Purpose: Considering the constraints of unknown external disturbances and internal modeling uncertainty, a robust controller is designed to realize the fly-around control of the space tumbling target. The relative distance of the LOS direction flies around the radius, and the LOS rotation rate is consistent with the target precession rate.

IV. UNITS DESIGN AND STABILITY ANALYSIS OF THE COMPOUND CONTROLLER

A. TRACKING DIFFERENTIATOR (TD)

TD [63], [64] is used to arrange the transition process for the desired signal, effectively solve the contradiction between overshoot and rapidity while realizing the purpose of tracking

the desired signal as soon as possible, and accurately extracting the differential signal of the desired signal. A TD has many forms, and its structure is usually divided into linear and nonlinear forms. For the relative motion equation in the RLOS coordinate system, the second-order TD is designed as follows:

$$\begin{cases} \boldsymbol{e}_0 = \boldsymbol{v}_1 - \boldsymbol{x}_\mathrm{d} \\ \dot{\boldsymbol{v}}_1 = \boldsymbol{v}_2 \\ \dot{\boldsymbol{v}}_2 = \mathrm{fhan}(\boldsymbol{e}_0, \boldsymbol{v}_2, m_0, h_0) \end{cases} \tag{11}$$

where $\boldsymbol{x}_\mathrm{d} = [r_\mathrm{d}, q_\mathrm{d}]^\mathrm{T} \in \mathbb{R}^2$ is the expected tracking signal of the system, r_d is the expected flying radius, q_d is the expected LOS angle, and v_1 is the tracking signal of the expected signal. $\dot{\boldsymbol{x}}_\mathrm{d} = [\dot{r}_\mathrm{d}, \dot{q}_\mathrm{d}]^T \in \mathbb{R}^2$ is the differential signal of the expected tracking signal of the system, $\dot{r}_\mathrm{d}$ is the expected relative speed, $\dot{q}_\mathrm{d}$ is the expected LOS rotation rate, and v_2 is the tracking signal of the expected differential signal. $\mathrm{fhan}\,(c_1, c_2, m_0, h_0)$ is the fastest control synthesis function [65] that can avoid high-frequency oscillations, where m_0 is the velocity factor, which determines the bandwidth of the tracking differentiator, and h_0 is the filtering factor, which corresponds to the integration step in the numerical simulation. The expression is as follows:

$$\begin{cases} d = m_0 h_0^2 \\ a_0 = h_0 c_2 \\ k = c_1 + a_0 \\ a_1 = \sqrt{d\,(d + 8\,|k|)} \\ a_2 = a_0 + \mathrm{sign}\,(k)\,(a_1 - d)/2 \\ a = (a_0 + k)\,\mathrm{fsg}\,(k, d) + a_2\,(1 - \mathrm{fsg}\,(k, d)) \\ \mathrm{fhan}\,(c_1, c_2, m_0, h_0) = -m_0\,(a/d)\,\mathrm{fsg}\,(a, d) - \\ m_0 \mathrm{sign}\,(a)\,(1 - \mathrm{fsg}\,(a, d)) \\ \mathrm{fsg}\,(x, d) = (\mathrm{sign}\,(x + d) - \mathrm{sign}\,(x - d))\,/2 \end{cases} \tag{12}$$

where the function of $\mathrm{fsg}\,(x, d)$ [65] is an equivalent formula derived using the characteristics of symbolic function and parameter reduction when two conditional statements appear at the same time.

B. NONLINEAR EXTENDED STATE OBSERVER (NLESO)

ESO [66]–[68] is the key link in the entire system. In this study, the external disturbance and uncertainty inside the system are reduced to "total disturbance," and expanded into new state variables $\boldsymbol{x}_3$ for real-time estimation and compensation. $\boldsymbol{x}_3$ is expressed as follows:

$$\boldsymbol{x}_3 = \boldsymbol{B}(\boldsymbol{F}(\boldsymbol{t}) + \boldsymbol{w}(\boldsymbol{t})) \in \mathbb{R}^2 \tag{13}$$

The third-order NLESO is designed as follows:

$$\begin{cases} \boldsymbol{e}_1 = \boldsymbol{z}_1 - \boldsymbol{y} \\ \dot{\boldsymbol{z}}_1 = \boldsymbol{z}_2 - \beta_{01}\boldsymbol{e}_1 \\ \dot{\boldsymbol{z}}_2 = f(\boldsymbol{z}_1, \boldsymbol{z}_2) + \boldsymbol{z}_3 - \beta_{02} g_1(\boldsymbol{e}_1) + \boldsymbol{B}\boldsymbol{u} \\ \dot{\boldsymbol{z}}_3 = -\beta_{03} g_2(\boldsymbol{e}_1) \end{cases} \tag{14}$$

where $\beta_{0i} \in \mathbb{R}(i = 1, 2, 3)$ are the parameters of the observer; $\boldsymbol{z}_1$, $\boldsymbol{z}_2$, and $\boldsymbol{z}_3$ are the estimated values of $\boldsymbol{x}_1$, $\boldsymbol{x}_2$, and $\boldsymbol{x}_3$, respectively; $f(\boldsymbol{z}_1, \boldsymbol{z}_2)$ is an estimate of $f(\boldsymbol{x}_1, \boldsymbol{x}_2)$; and the nonlinear function $g_i(\boldsymbol{e}_1)(i = 1, 2)$ select the functions of $\mathrm{fal}\,(\boldsymbol{e}_1, \alpha_i, \delta)$ [69], [70] which can effectively avoid the occurrence of high-frequency flutter as follows:

$$\mathrm{fal}\,(\boldsymbol{e}_1, \alpha_i, \delta) = \begin{cases} |\boldsymbol{e}_1|^{\alpha_i}\,\mathrm{sign}\,(\boldsymbol{e}_1), & |\boldsymbol{e}_1| > \delta \\ \boldsymbol{e}_1 \Big/ \delta^{1-\alpha_i}, & |\boldsymbol{e}_1| \le \delta \end{cases} \quad (i = 1, 2) \tag{15}$$

The nonlinear function $\mathrm{fal}\,(\boldsymbol{e}_1, \alpha_i, \delta)$ has characteristics of "small error, large gain; large error, small gain" when the degree of nonlinearity of the function $0 < \alpha_i < 1$. When $\alpha_i = 1$, the nonlinear function $\mathrm{fal}\,(\boldsymbol{e}_1, \alpha_i, \delta)$ turns into a linear one, Eq.(14) is called LESO [71], [72]. The parameter $\delta > 0$ represents the interval length of the linear segment.

C. IMPROVED NONLINEAR STATE ERROR FEEDBACK LAW (NLSEF)

Based on the idea of "error elimination error," considering the form of the classical ADRC error feedback control law and the characteristics that the traditional SMC is prone to chattering and steady-state error, the integral sliding mode surface function is selected in NLSEF in Eq. (16), and its derivative is given by Eq. (17).

$$\boldsymbol{s} = \begin{bmatrix} s_1 \\ s_2 \end{bmatrix} = \begin{bmatrix} \dot{e}_1 + \lambda_{21} e_1 + \lambda_{11} \int e_1 dt \\ \dot{e}_2 + \lambda_{22} e_2 + \lambda_{12} \int e_2 dt \end{bmatrix} \in \mathbb{R}^2 \tag{16}$$

$$\dot{\boldsymbol{s}} = \ddot{\boldsymbol{e}} + \boldsymbol{\lambda}_2 \dot{\boldsymbol{e}} + \boldsymbol{\lambda}_1 \boldsymbol{e} \tag{17}$$

where s_1 and s_2 are the sliding mode surface functions for LOS direction and vertical LOS direction selection, respectively. $\boldsymbol{\lambda}_i = \mathrm{diag}\,\{\lambda_{i1}, \lambda_{i2}\} \in \mathbb{R}^{2\times 2}$, $\lambda_{i1} > 0$, and $\lambda_{i2} > 0$, $i = 1$ and $i = 2$ are the proportional gain and differential gain, respectively. $\dot{\boldsymbol{e}} = \boldsymbol{v}_2 - \boldsymbol{z}_2 = \begin{bmatrix} \dot{e}_1 & \dot{e}_2 \end{bmatrix}^T \in \mathbb{R}^2$ and $\boldsymbol{e} = \boldsymbol{v}_1 - \boldsymbol{z}_1 = \begin{bmatrix} e_1 & e_2 \end{bmatrix}^T \in \mathbb{R}^2$ are system state errors.

Combined with the relative motion in Eq. (10) and Eq. (17) can be rewritten as follows:

$$\dot{\boldsymbol{s}} = f\,(\boldsymbol{x}_1, \boldsymbol{x}_2) + \boldsymbol{B}(\boldsymbol{F}(t) + \boldsymbol{w}(t) + \boldsymbol{u}) + \boldsymbol{\lambda}_2 \dot{\boldsymbol{e}} + \boldsymbol{\lambda}_1 \boldsymbol{e} \tag{18}$$

The exponential approach law with finite-time convergence term is selected as follows:

$$\dot{\boldsymbol{s}} = \boldsymbol{s} - \boldsymbol{\varepsilon} \begin{bmatrix} \mathrm{sgn}\, s_1 \\ \mathrm{sgn}\, s_2 \end{bmatrix} - \boldsymbol{\beta} \begin{bmatrix} |s_1|^{\eta_1}\,\mathrm{sgn}\, s_1 \\ |s_2|^{\eta_2}\,\mathrm{sgn}\, s_2 \end{bmatrix} \tag{19}$$

where $\boldsymbol{\varepsilon} = \mathrm{diag}\,\{\varepsilon_1, \varepsilon_2\} \in \mathbb{R}^{2\times 2}, \varepsilon_i > 0 (i = 1, 2)$, $\boldsymbol{\beta} = diag\,\{\beta_1, \beta_2\} \in \mathbb{R}^{2\times 2}$, $\beta_{\min} = \min\{\beta_1, \beta_2\}$, $\beta_i > 0 (i = 1, 2)$, and $\boldsymbol{\eta}_0 = [\eta_1, \eta_2]^T \in \mathbb{R}^2$, $\eta_{\min} = \min\{\eta_1, \eta_2\}$, $-1 < \eta_i < 1$ $(i = 1, 2)$ are undetermined coefficients.

Combining Eq. (18) and Eq. (19) is expressed as follows:

$$\begin{aligned} \boldsymbol{u}' = -\boldsymbol{B}^{-1}(&\boldsymbol{\varepsilon} \begin{bmatrix} \mathrm{sgn}\, s_1 \\ \mathrm{sgn}\, s_2 \end{bmatrix} + \boldsymbol{\beta} \begin{bmatrix} |s_1|^{\eta_1}\,\mathrm{sgn}\, s_1 \\ |s_2|^{\eta_2}\,\mathrm{sgn}\, s_2 \end{bmatrix} \\ &+ \lambda_1 \dot{\boldsymbol{e}} + \lambda_0 \boldsymbol{e} + f(\boldsymbol{x}_1, \boldsymbol{x}_2) + \boldsymbol{F}(t) + \boldsymbol{w}(t)) \end{aligned} \tag{20}$$

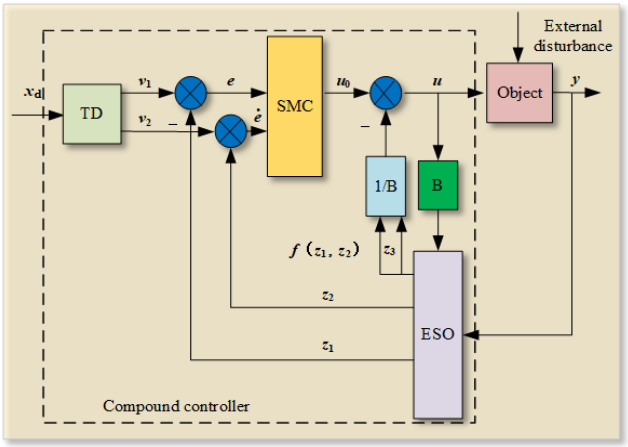

FIGURE 3. The block diagram of the compound controller.

The NLSEF is as follows:

$$\boldsymbol{u}_0 = -\boldsymbol{B}^{-1}(\boldsymbol{\varepsilon}\begin{bmatrix}\operatorname{sgn} s_1\\ \operatorname{sgn} s_2\end{bmatrix} + \boldsymbol{\beta}\begin{bmatrix}|s_1|^{\eta_1}\operatorname{sgn} s_1\\ |s_2|^{\eta_2}\operatorname{sgn} s_2\end{bmatrix} + \boldsymbol{\lambda}_2\dot{\boldsymbol{e}} + \boldsymbol{\lambda}_1\boldsymbol{e}) \tag{21}$$

The NLSEF after compensation is as follows:

$$\boldsymbol{u} = -\boldsymbol{B}^{-1}(\boldsymbol{\varepsilon}\begin{bmatrix}\operatorname{sgn} s_1\\ \operatorname{sgn} s_2\end{bmatrix} + \boldsymbol{\beta}\begin{bmatrix}|s_1|^{\eta_1}\operatorname{sgn} s_1\\ |s_2|^{\eta_2}\operatorname{sgn} s_2\end{bmatrix} + \boldsymbol{\lambda}_2\dot{\boldsymbol{e}} + \boldsymbol{\lambda}_1\boldsymbol{e} + f(z_1, z_2) + z_3) \tag{22}$$

The structural diagram of the controller is shown in Fig. 3.

D. CONVERGENCE AND STABILITY ANALYSIS

First, the convergence of the ESO in the controller is analyzed. The initial values of the error term and $f(\boldsymbol{x}_1, \boldsymbol{x}_2, t)$ assumed to be zero. The equivalent gain method is adopted The $g_1(\boldsymbol{e}_1)$ and $g_2(\boldsymbol{e}_1)$ in Eq. (14) can be expressed as follows:

$$\begin{aligned} g_i(\boldsymbol{e}_1) &= \operatorname{fal}(\boldsymbol{e}_1, \alpha_i, \delta)\\ &= \frac{\operatorname{fal}(\boldsymbol{e}_1, \alpha_i, \delta)}{\boldsymbol{e}_1}\boldsymbol{e}_1\\ &= \zeta_{0i}(\boldsymbol{e}_1)\boldsymbol{e}_1, \quad i = 1, 2 \end{aligned} \tag{23}$$

Thus, $g_i(\boldsymbol{e}_1)$ can be seen as a linear function $\boldsymbol{e}_1$ with varying gain $\zeta_{0i}(\boldsymbol{e}_1)$ [72].

Assuming:

$$\lambda_{0i} = \zeta_{0i}(\boldsymbol{e}_1), \quad i = 1, 2 \tag{24}$$

Eq. (14) of NLESO can be rewritten as follows:

$$\begin{cases} \boldsymbol{e}_1 = z_1 - \boldsymbol{y}\\ \dot{z}_1 = z_2 - \beta_{01}\boldsymbol{e}_1\\ \dot{z}_2 = z_3 - \beta_{02}\lambda_{01}\boldsymbol{e}_1 + \boldsymbol{B}_0\boldsymbol{u}\\ \dot{z}_3 = -\beta_{03}\lambda_{02}\boldsymbol{e}_1 \end{cases} \tag{25}$$

The transfer function from input to output is as follows:

$$z_1 = \frac{\beta_{01}s^2 + \beta_{02}\lambda_{01}s + \beta_{03}\lambda_{02}}{s^3 + \beta_{01}s^2 + \beta_{02}\lambda_{01}s + \beta_{03}\lambda_{02}}\boldsymbol{y}$$

$$\begin{aligned} z_2 &= \frac{\beta_{02}\lambda_{01}s^2 + \beta_{03}\lambda_{02}s}{s^3 + \beta_{01}s^2 + \beta_{02}\lambda_{01}s + \beta_{03}\lambda_{02}}\boldsymbol{y}\\ z_3 &= \frac{\beta_{03}\lambda_{02}s^2}{s^3 + \beta_{01}s^2 + \beta_{02}\lambda_{01}s + \beta_{03}\lambda_{02}}\boldsymbol{y} \end{aligned} \tag{26}$$

The characteristic equation is as follows:

$$s^3 + s^2\beta_{01} + s\beta_{02}\lambda_{01} + \beta_{03}\lambda_{02} \tag{27}$$

According to the root locus method, if the characteristic roots of characteristic Eq. (27) are located on the left side of the [S] plane and the system is stable. However, because of the gains λ_{01} and λ_{02} change with the size of the error $\boldsymbol{e}_1$, the root-finding process becomes complex. According to the specific physical process, the trajectory of the system closed-loop characteristic root moving with $\boldsymbol{e}_1$ on the [S] plane must be determined, and the stability is judged according to the distribution of characteristic roots. Therefore, if the appropriate observer gains β_{01}, β_{02}, and β_{03} should be selected such that the eigenvalues of the characteristic Eq. (27) are located on the left side of the [S] plane, the ESO is convergent and can estimate and compensate the state variables and "total disturbance" in realtime.

Secondly, the stability of the closed-loop system is proved.

Lemma 1 [73]: Consider the system $\dot{\boldsymbol{x}} = f(\boldsymbol{x})$, $\boldsymbol{x} \in \mathbb{R}^n$, $\forall \boldsymbol{x}(0)$, if there exists a continuous Lyapunov function $V(\boldsymbol{x}) \geq 0$ in $\mathbb{R}^n$, and scalars $c_1 > 0$, $\chi > 0$, $0 < p < 1$, such that

$$\dot{V}(\boldsymbol{x}) \leq -c_1 V^p(\boldsymbol{x}) + \chi \tag{28}$$

Then, the system $\dot{\boldsymbol{x}} = f(\boldsymbol{x})$ is the global practical finite-time bounded (GPFB), and the trajectory of the closed-loop system converges to a compact set containing the origin in a finite time T, $\lim_{t\to T}\boldsymbol{x} \in \left\{\boldsymbol{x} : V^p(\boldsymbol{x}) \leq \frac{\chi}{(1-q)c_1}\right\}$. The settling time T is given as Eq. (29), $0 < q < 1$ is a scalar, and $V(\boldsymbol{x}(0))$ is the initial value of $V(\boldsymbol{x})$.

$$T = \frac{1}{(1-p)qc_1}\left[V^{1-p}(x(0)) - \left(\frac{\chi}{(1-q)c_1}\right)^{(1-p)/p}\right] \tag{29}$$

Lemma 2 [74]: For any variables $x_i \in \mathbb{R}$, $i = 1, \cdots, n$, and a real number $p \in (0, 1]$, there is inequalitie

$$\begin{aligned} (|x_1| + \cdots + |x_n|)^p &\leq |x_1|^p + \cdots + |x_n|^p\\ &\leq n^{1-p}(|x_1| + \cdots + |x_n|)^p \end{aligned} \tag{30}$$

Lemma 3 [75]: For variables $x, y \in \mathbb{R}$, there exists $\alpha > 0$, and scalars $p > 1$, $q > 1$, $(q-1)(p-1) = 1$, there is inequalitie

$$xy \leq \frac{\alpha^p}{p}|x|^p + \frac{1}{q\alpha^q}|y|^q \tag{31}$$

Theorem 1: For the system Eq.(10) satisfying Assumption 2-3, the NLSEF in Eq.(22) will guarantee the the system is GPFB property of the closed-loop system if the design parameters are selected appropriately.

Proof: The positive-definite candidate of the Lyapunov function is selected as follows:

$$V = 1/2 s^{\mathrm{T}} s \tag{32}$$

We take the derivative of Eq. (32), and substitute Eq. (17) and Eq. (22) into it as follows:

$$\begin{aligned}
\dot{V} &= \boldsymbol{s}^{\mathrm{T}}\dot{\boldsymbol{s}} \\
&= \boldsymbol{s}^{T}\left(\ddot{\boldsymbol{e}} + \lambda_2\dot{\boldsymbol{e}} + \lambda_1\boldsymbol{e}\right) \\
&= \boldsymbol{s}^{T}\left(\dot{\boldsymbol{x}}_2 + \lambda_2\dot{\boldsymbol{e}} + \lambda_1\boldsymbol{e}\right) \\
&= \boldsymbol{s}^{T}[f(\boldsymbol{x}_1,\boldsymbol{x}_2) + \boldsymbol{B}\left(\boldsymbol{F}(t) + \boldsymbol{w}(t) + \boldsymbol{u}\right) + \lambda_2\dot{\boldsymbol{e}} + \lambda_1\boldsymbol{e}] \\
&= \boldsymbol{s}^{T}[f(\boldsymbol{x}_1,\boldsymbol{x}_2) + \boldsymbol{B}(\boldsymbol{F}(t) + \boldsymbol{w}(t)) + \lambda_2\dot{\boldsymbol{e}} + \lambda_1\boldsymbol{e} \\
&\quad - \varepsilon\begin{bmatrix}\operatorname{sgn} s_1 \\ \operatorname{sgn} s_2\end{bmatrix} - \beta\begin{bmatrix}|s_1|^{\eta_1}\operatorname{sgn} s_1 \\ |s_2|^{\eta_2}\operatorname{sgn} s_2\end{bmatrix} \\
&\quad - f(\boldsymbol{z}_1,\boldsymbol{z}_2) - \boldsymbol{z}_3 - \lambda_2\dot{\boldsymbol{e}} - \lambda_1\boldsymbol{e}]
\end{aligned} \tag{33}$$

In the case of bounded total interference, the observation error is bounded, and the value depends on the parameters of ESO [65]. It is assumed that ζ_1 and ζ_2 are observation errors in the LOS direction and vertical LOS direction, respectively. Let, $\boldsymbol{\zeta} = [\zeta_1, \zeta_2]^T \in \mathbb{R}^2$, the observation error is as follows:

$$\boldsymbol{B}(\boldsymbol{F}(t) + \boldsymbol{w}(t)) + f(\boldsymbol{x}_1,\boldsymbol{x}_2) - \boldsymbol{z}_3 - f(\boldsymbol{z}_1,\boldsymbol{z}_2) = \zeta \tag{34}$$

Then

$$\begin{aligned}
\dot{V} &= \boldsymbol{s}^{\mathrm{T}}[-\varepsilon\begin{bmatrix}\operatorname{sgn} s_1 \\ \operatorname{sgn} s_2\end{bmatrix} - \beta\begin{bmatrix}|s_1|^{\eta_1} & 0 \\ 0 & |s_2|^{\eta_2}\end{bmatrix}\begin{bmatrix}\operatorname{sgn} s_1 \\ \operatorname{sgn} s_2\end{bmatrix} + \zeta] \\
&\le \boldsymbol{s}^{\mathrm{T}}[-\beta\begin{bmatrix}|s_1|^{\eta_1} & 0 \\ 0 & |s_2|^{\eta_2}\end{bmatrix}\begin{bmatrix}\operatorname{sgn} s_1 \\ \operatorname{sgn} s_2\end{bmatrix} + \zeta] \\
&= -2^{\frac{\eta_1+1}{2}}\beta_1\left|\frac{1}{2}s_1^2\right|^{\frac{\eta_1+1}{2}} - 2^{\frac{\eta_2+1}{2}}\beta_2\left|\frac{1}{2}s_2^2\right|^{\frac{\eta_2+1}{2}} + \boldsymbol{s}^{\mathrm{T}}\zeta \\
&\le -2^{\frac{\eta_{\min}+1}{2}}\beta_{\min}\left(\left|\frac{1}{2}s_1^2\right|^{\frac{\eta+1}{2}} + \left|\frac{1}{2}s_2^2\right|^{\frac{\eta+1}{2}}\right) + \boldsymbol{s}^{\mathrm{T}}\zeta
\end{aligned} \tag{35}$$

When the values of s_1 and s_2 change, the value of η is η_1 or η_2, which satisfies the inequality as follows:

$$\left|\frac{1}{2}s_1^2\right|^{\frac{\eta_1+1}{2}} + \left|\frac{1}{2}s_2^2\right|^{\frac{\eta_2+1}{2}} \ge \left|\frac{1}{2}s_1^2\right|^{\frac{\eta+1}{2}} + \left|\frac{1}{2}s_2^2\right|^{\frac{\eta+1}{2}} \tag{36}$$

According to Lemma 2, there is inequalitie

$$\begin{aligned}
&-2^{\frac{\eta_{\min}+1}{2}}\beta_{\min}\left(\left|\frac{1}{2}s_1^2\right|^{\frac{\eta+1}{2}} + \left|\frac{1}{2}s_2^2\right|^{\frac{\eta+1}{2}}\right) \\
&\le -2^{\frac{\eta_{\min}+1}{2}}\beta_{\min}\left(\left|\frac{1}{2}s_1^2\right| + \left|\frac{1}{2}s_2^2\right|\right)^{\frac{\eta+1}{2}}
\end{aligned} \tag{37}$$

According to Lemma 3, there is inequalitie

$$\boldsymbol{s}^{\mathrm{T}}\zeta \le \frac{\varepsilon^{\eta+1}}{\eta+1}\|\boldsymbol{s}\|^{\eta+1} + \frac{\eta}{(\eta+1)\varepsilon^{\frac{\eta+1}{\eta}}}\|\zeta\|^{\frac{\eta+1}{\eta}} \tag{38}$$

where $\varepsilon > 0$.

Substituting Eq. (37) and Eq. (38) into Eq. (35) is expressed as follows:

$$\begin{aligned}
\dot{V} &\le -2^{\frac{\eta_{\min}+1}{2}}\beta_{\min}\left(\left|\frac{1}{2}s_1^2\right| + \left|\frac{1}{2}s_2^2\right|\right)^{\frac{\eta+1}{2}} + \frac{\varepsilon^{\eta+1}}{\eta+1}\|\boldsymbol{s}\|^{\eta+1} \\
&\quad + \frac{\eta}{(\eta+1)\varepsilon^{\frac{\eta+1}{\eta}}}\|\boldsymbol{\zeta}\|^{\frac{\eta+1}{\eta}} \\
&= -2^{\frac{\eta_{\min}+1}{2}}\beta_{\min}V^{\frac{\eta+1}{2}} + 2^{\frac{\eta+1}{2}}\frac{\varepsilon^{\eta+1}}{\eta+1}V^{\frac{\eta+1}{2}} \\
&\quad + \frac{\eta}{(\eta+1)\varepsilon^{\frac{\eta+1}{\eta}}}\|\boldsymbol{\zeta}\|^{\frac{\eta+1}{\eta}} \\
&= -(2^{\frac{\eta_{\min}+1}{2}}\beta_{\min} - 2^{\frac{\eta+1}{2}}\frac{\varepsilon^{\eta+1}}{\eta+1})V^{\frac{\eta+1}{2}} \\
&\quad + \frac{\eta}{(\eta+1)\varepsilon^{\frac{\eta+1}{\eta}}}\|\boldsymbol{\zeta}\|^{\frac{\eta+1}{\eta}}
\end{aligned} \tag{39}$$

Take $\beta_{\min}$ satisfying $\beta_{\min} \ge 2^{\frac{\eta-\eta_{\min}}{2}}\frac{\varepsilon^{\eta+1}}{\eta+1} + \frac{1}{2^{\frac{\eta_{\min}+1}{2}}}\phi$, where, ϕ is a positive constant, Eq. (39) can be rewritten as

$$\dot{V} \le -\phi V^{\frac{\eta+1}{2}} + \frac{\eta}{(\eta+1)\varepsilon^{\frac{\eta+1}{\eta}}}\|\zeta\|^{\frac{\eta+1}{\eta}} \tag{40}$$

According to the definition of V and Lemma 1, the trajectories of the closed-loop system would converge into a small set containing the origin point in finite time. The integral sliding mode surface $\boldsymbol{s}$ fall into and remain in the attractive set $\Omega := \left\{\boldsymbol{s} : \|\boldsymbol{s}\|^{\eta+1} \le 2^{\frac{\eta+1}{2}}B_0\right\}$, B_0 is a positive constant as Eq.(41), where $0 < q < 1$. B_0 could be small enough by adjusting parameters appropriately. The settling time can be obtained as follows as Eq.(42).

$$B_0 = \frac{\eta}{(1-q)\phi(\eta+1)\varepsilon^{\frac{\eta+1}{\eta}}}\|\zeta\|^{\frac{\eta+1}{\eta}} \tag{41}$$

$$T = \frac{2}{(1-\eta)q\phi}\left[V^{\frac{1-\eta}{2}}(x(0)) - B_0^{\frac{1-\eta}{1+\eta}}\right] \tag{42}$$

V. SIMULATION VERIFICATION

The initial parameters of the tumbling target and tracking spacecraft are presented in Table 1.

The initial relative distance, initial relative speed, initial LOS angle, and initial LOS rotation rate are as follows: $r_0 = 60$ m, $v_0 = 5.2 \times 10^{-4}$ m/s, $q_0 = 1$ rad, and $\dot{q} = 1.8 \times 10^{-3}$ rad/s, respectively. The expected relative distance, relative speed, LOS angle, and LOS rotation rate are: $r_{\mathrm{d}} = 50$ m, $v_{\mathrm{d}} = 0$ m/s, $q_{\mathrm{d}} = q_0 + \dot{q}_{\mathrm{d}}t$, and $\dot{q}_d = 3.92 \times 10^{-2}$ rad/s, respectively. It is assumed that the maximum control force provided by the actuator of the tracking spacecraft in the LOS direction and vertical LOS direction are: $\mathrm{U}_{r\,\max} = 0.4$ N and $\mathrm{U}_{q\,\max} = 2$ N, respectively. The parameters of the controller are set as follows: the integral step size h is 0.0001; m_0 and h_0 involved in TD are 0.08 and 0.001 respectively; β_{01}, β_{02}, and β_{03} in ESO are 100, 1000, and 10000 respectively, and nonlinear functions are $g_1(\boldsymbol{e}_1) = \mathrm{fal}(\boldsymbol{e}_1, 0.5, h)$ and $g_2(\boldsymbol{e}_1) = \mathrm{fal}(\boldsymbol{e}_1, 0.25, h)$; In NLSEF, the proportional gain and differential gain λ_0 and λ_1 are set to 5, ε, β, and η are set to 0.0001, 0.01, and 0.5 respectively.

To verify that the controller designed in this study has strong robustness to external unknown disturbances and internal modeling uncertainty, a simulation comparison is carried out under the four conditions of "total disturbance:" step

TABLE 1. Initial parameters.

Name	Parameter	Parameter value
Tumbling target	Semimajor axis	7078140 m
	Eccentricity	0
	True anomaly	30 deg
	Inclination	68 deg
	The right ascension of ascending node	0 deg
	Argument of perigee	60 deg
	Nutation angle rate	0 rad/s
	Precession angle rate	0.0392 rad/s
	Self-rotation angle rate	0.0274 rad/s
Tracking spacecraft	Relative position	28.19 m
		20.52 m
		48.83 m
	Relative velocity	3.5×10^{-4} m/s
		2×10^{-4} m/s
		3.3×10^{-4} m/s

disturbance, sinusoidal disturbance, uniformly distributed random disturbance, and no disturbance. It should be noted that according to the relative motion equation and the characteristics of the ESO, the disturbance in the vertical LOS direction is set as the ratio of "total disturbance" to the relative distance in the LOS direction. Among them, step disturbance: the disturbance in the value of $w_r = 0.05$ m/s^2 and $w_\theta/r = 0.01$ m/s^2 occurs at 25 s; sinusoidal disturbance: $w_r = 0.05\sin(\pi t)$ m/s^2 and $w_\theta/r = 0.01\sin(\pi t + \pi/2)$ m/s^2; the uniformly distributed random disturbance is a uniform random distribution function whose amplitude satisfies 0.05 m/s^2 and 0.01 m/s^2 respectively.

A. ESO CONVERGENCE AND OBSERVATION EFFECT SIMULATION VERIFICATION

Before studying the control problem with multiple constraints, the convergence of the ESO is verified by simulation when the "total disturbance" is sinusoidal. Fig. 4 shows the error root locus in the LOS direction and vertical LOS direction. It can be seen that when the error system changes with $\boldsymbol{e}_1$, the closed-loop pole is always located on the left half-plane of [S]; that is, any $\boldsymbol{e}_1$ value system gradually tends to equilibrium, and the ESO has good convergence.

Fig. 5 shows the estimation of sinusoidal disturbance by ESO. It can be seen that the estimation error is small and there is only a small phase lag.

B. COMPARATIVE SIMULATION VERIFICATION

To further prove the superiority of the controller designed in this study, a compound controller is simulated and compared with traditional SMC. As shown in Fig. 6, within the acceptable overshoot range, the controller designed in this study can converge to the expected value faster by adjusting the TD parameters. As shown in Fig. 7, the compound controller designed in this study overcomes the chattering problem of the traditional SMC in both LOS and vertical LOS directions. For quantitative purposes, six popular performance specifications are employed to evaluate the control performance: the rise time, overshoot, settling time, mean absolute error

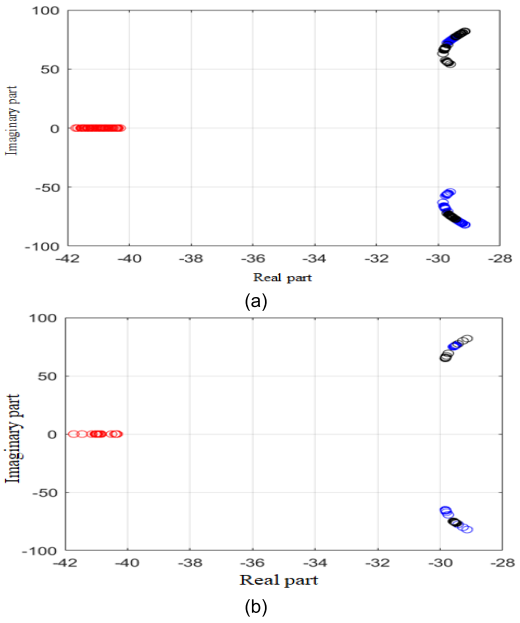

FIGURE 4. Root locus of error. (a) Root locus of the LOS direction error. (b) Root locus of the vertical LOS direction error.

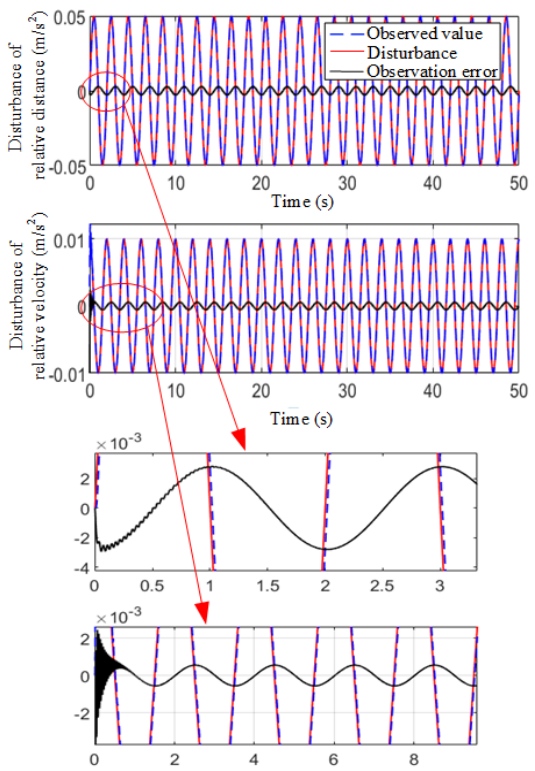

FIGURE 5. Sinusoidal disturbance tracking effect.

(MAE), mean absolute control input (MAI) and mean total variation (MTV) of the control [76]. The expressions for the last three performance specifications are as follows:

$$\mathrm{MAE} = \frac{1}{t_\infty - t_0}\int_{t_0}^{t_\infty} |e(t)|\mathrm{d}t$$

TABLE 2. Performance comparison of the compound controller and the traditional SMC.

Name	Compound controller				Traditional SMC			
	LOS direction		Vertical LOS direction		LOS direction		Vertical LOS direction	
	Relative distance	Relative speed	LOS angle	LOS rotation rate	Relative distance	Relative speed	LOS angle	LOS rotation rate
Rise time	21.735 s	22.362 s	4.760 s	6.801 s	58.726 s	59.238 s	64.556 s	68.661 s
Overshoot	0 m	0.8992 m/s	0 rad	0.3112 rad/s	0 m	0.3842 m/s	0 rad	0.0405 rad/s
Settling time	14.435 s	21.734 s	0 s	2.850 s	24.452 s	41.722 s	0 s	1.404 s
MAE	1.1192	2.9545	3.0600	3.3007×10^{-4}	1.6910	2.9590	3.0600	5.2396×10^{-4}
MAI	0.0889		0.5934		0.0897		0.5403	
MTV	3.6215×10^{-5}		0.0040		2.9783×10^{-4}		1.0188	

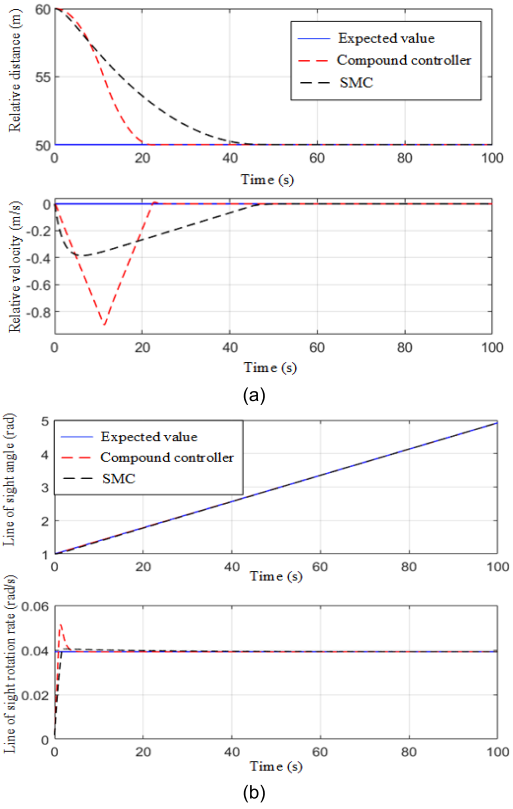

FIGURE 6. Comparison curves between the compound controller and the traditional controller. (a) Variation curves in the LOS direction. (b) Variation curves in the vertical LOS direction.

$$\mathrm{MAI} = \frac{1}{t_\infty - t_0}\int_{t_0}^{t_\infty} |u(t)|\mathrm{d}t$$
$$\mathrm{MTV} = \frac{1}{t_\infty - t_0}\int_{t_0}^{t_\infty} |u(t+1) - u(t)|\mathrm{d}t \qquad (43)$$

A quantitative comparison of the control performances is presented in Table 2. Note that the overshoot, settling time for the LOS rotation rate, and MAI for the LOS rotation rate (underlined in Table 2) are observed to be larger under the compound controller than under the traditional SMC. Even so, the compound controller is more reasonable when evaluating the performance indices from the overall point of view. System response is preferred in practice, considering

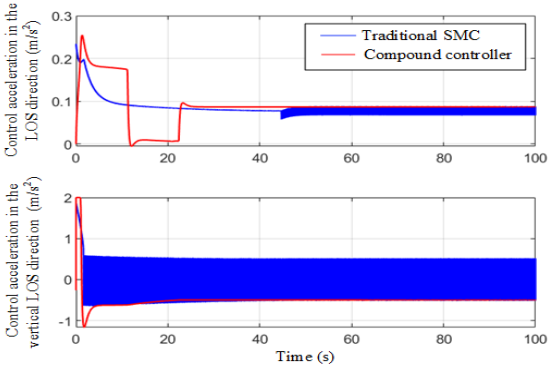

FIGURE 7. The acceleration comparison between the compound controller and the traditional SMC.

the convergence response, disturbance rejection, energy consumption, and control curve smoothness.

C. SIMULATION VERIFICATION UNDER MULTIPLE CONSTRAINTS

Considering the existence of unknown external disturbances, internal unmodeled dynamics, and limited saturation of the control input, the variation curves of the spacecraft fly-around radius, relative speed in the LOS direction, LOS angle, and LOS rotation rate with time under the action of the compound controller designed in this study are shown in Fig. 8. Under the four disturbance conditions, the tracking spacecraft can track the desired radius within 25 s and remain stable; the relative velocity in the LOS direction first increases and then decreases, and converges to 0 when the relative distance in the LOS direction reaches the expected value; the LOS angle reaches the desired curve within 5 s and tracks stably; the LOS rotation rate first increases and then decreases, and converges to near 0.039 m/s after the LOS angle reaches the desired curve. From the locally enlarged view of the relative speed in the LOS direction and the LOS rotation rate, it can be observed that the control effect is slightly affected by the disturbance, and the control quality under different disturbances remains unchanged, which shows that the controller designed in this study has strong robustness.

Considering the existence of unknown external disturbances, internal unmodelled dynamics, and limited saturation

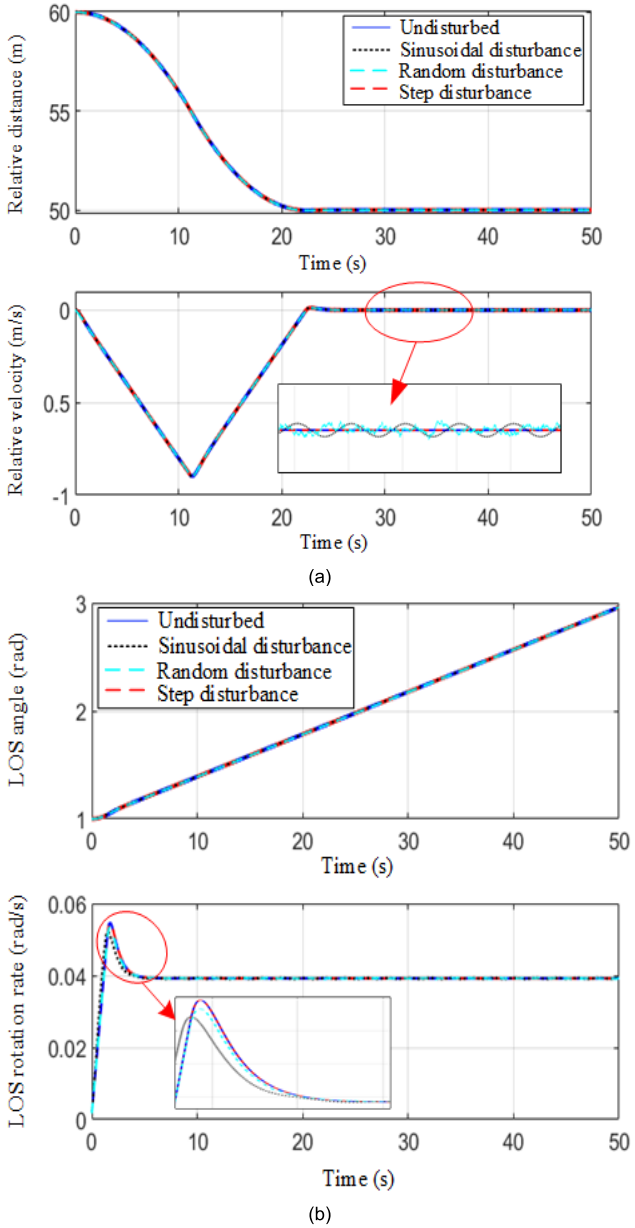

FIGURE 8. Comparison curves under four "total disturbances." (a) Variation curves in the LOS direction. (b) Variation curves in the vertical LOS direction.

of the control input, the change curves of the control acceleration in the LOS and vertical LOS directions are shown in Fig. 9. At the initial stage, they are limited by actuator saturation, but with a reduction in the control error, the saturation phenomenon gradually disappears, and finally achieves the purpose of control. It should be noted that when the "total disturbance" is a random disturbance, because of the phase lag in the estimation of the random disturbance, the random disturbance cannot be directly used to compensate for the control acceleration. In this study, the upper bound of the random disturbance estimation is used to compensate for the control acceleration, and the compensated

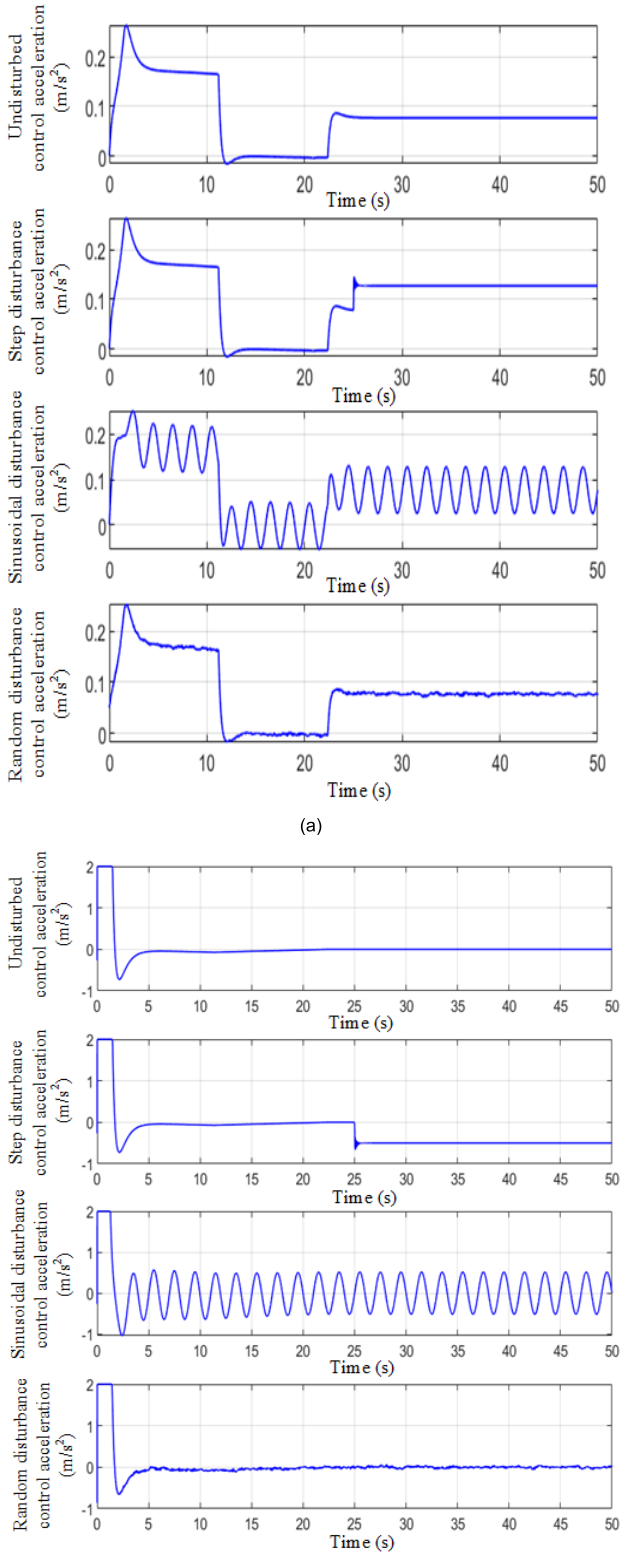

FIGURE 9. Control curves under four "total disturbance." (a) Control acceleration in the LOS direction. (b) Control acceleration in the vertical LOS direction.

control acceleration oscillates within an acceptably small range.

VI. CONCLUSION

Considering the on-orbit service task of a space tumbling target as the research background, this study investigates the short-range relative motion control of a space tumbling target under multiple constraints. The relative orbit dynamics model in the RLOS coordinate system is derived to solve the control problem of space tumbling target fly-around under the constraints of external unknown disturbances and internal modeling uncertainty. In this study, ADRC and SMC are combined to design a compound controller, which realizes the real-time estimation and compensation of "total disturbance," reduces the steady-state error of the system, overcomes the chattering problem of the traditional SMC, and effectively improves the robustness of the system. The simulation results show that, under the four conditions of no disturbance, step disturbance, sinusoidal disturbance, and random disturbance, the controller designed in this study can track and compensate for the disturbance in real time, ensure good control quality, and have strong robustness to external disturbances and internal modeling uncertainty. After reasonably arranging the transition process, the sensitivity of the control law to parameters decreases, and the adjustable range of parameters is large, which is a control method that is easy for engineering practice.

REFERENCES

[1] R. Miller, "Orbital debris quarterly news," NASA, Washington, DC, USA, Tech. Rep. 4, vol. 25, Dec. 2021. [Online]. Available: http://ufdc.ufl.edu/AA00058853/00095
[2] S. Bandyopadhyay, S.-J. Chung, and F. Y. Hadaegh, "Nonlinear attitude control of spacecraft with a large captured object," *J. Guid., Control, Dyn.*, vol. 39, no. 4, pp. 754–769, Apr. 2016, doi: 10.2514/1.G001341.
[3] L. Zhang, S. Qian, S. Zhang, and H. Cai, "Research on angles-only/SINS/CNS relative position and attitude determination algorithm for a tumbling spacecraft," *Proc. Inst. Mech. Eng. G, J. Aerosp. Eng.*, vol. 231, no. 2, pp. 218–228, Feb. 2017, doi: 10.1177/095441.0016636153.
[4] Y. She, J. Sun, S. Li, W. Li, and T. Song, "Quasi-model free control for the post-capture operation of a non-cooperative target," *Acta Astronautica*, vol. 147, pp. 59–70, Jun. 2018, doi: 10.1016/j.actaastro.2018.03.041.
[5] M. Wang, J. Luo, J. Yuan, and U. Walter, "Detumbling strategy and coordination control of kinematically redundant space robot after capturing a tumbling target," *Nonlinear Dyn.*, vol. 92, no. 3, pp. 1023–1043, May 2018, doi: 10.1007/s11071-018-4106-4.
[6] Q. Hu, W. Chen, and L. Guo, "Fixed-time maneuver control of spacecraft autonomous rendezvous with a free-tumbling target," *IEEE Trans. Aerosp. Electron. Syst.*, vol. 55, no. 2, pp. 562–577, Apr. 2019, doi: 10.1109/TAES.2018.2852439.
[7] X. Ding, Y. Wang, Y. Wang, and K. Xu, "A review of structures, verification, and calibration technologies of space robotic systems for on-orbit servicing," *Sci. China Technol. Sci.*, vol. 64, no. 3, pp. 462–480, Mar. 2021, doi: 10.1007/s11431-020-1737-4.
[8] A. Flores-Abad, O. Ma, K. Pham, and S. Ulrich, "A review of space robotics technologies for on-orbit servicing," *Prog. Aerosp. Sci.*, vol. 68, pp. 1–26, Jul. 2014, doi: 10.1016/j.paerosci.2014.03.002.
[9] M. H. Shan, J. Guo, and E. Gill, "Review and comparison of active space debris capturing and removal methods," *Prog. Aerosp. Sci.*, vol. 80, pp. 18–32, Jan. 2016, doi: 10.1016/j.paerosci.2015.001.
[10] H. D. Liu, X. Q. Wang, B. Liang, F. Wen, Y. Xu, and Y. Shi, "Motion characteristics analysis and ground simulation method of spin target in autonomous capture," *Robot*, vol. 35, no. 1, pp. 1–8, Jan. 2013, doi: 10.3724/SP.J.1218.2013.00001.
[11] J. Luo, L. Zong, M. Wang, and J. Yuan, "Optimal capture occasion determination and trajectory generation for space robots grasping tumbling objects," *Acta Astronautica*, vol. 136, pp. 380–386, Jul. 2017, doi: 10.1016/j.actaastro.2017.03.026.
[12] Y. X. Hao, L. Shen, and Y. Li, "Assortment of tumbling objects in space and movement characteristics analysis," *Missiles Space Vehicles*, vol. 5, Feb. 2018, pp. 57–63, doi: 10.7654/j.issn.1004-7182.20180512.
[13] X. Peng, X. Shi, and Y. Gong, "Integrated modeling of spacecraft relative motion dynamics using dual quaternion," *J. Syst. Eng. Electron.*, vol. 29, no. 2, pp. 367–377, Apr. 2018, doi: 10.21629/JSEE.2018.02.17.
[14] Y. X. Hao, L. Shen, and Y. Li, "The simulation of tumbling objects in space and movement characteristics analysis," *Missiles Space Vehicles*, vol. 1, pp. 74–79, Summer 2019, doi: 10.7654/j.issn.1004-7182.20190116.
[15] J. Y. Wang, H. C. Liang, and Z. W. Sun, "Dual number-based relative coupled dynamics and control," *J. Astronaut.*, vol. 31, no. 7, pp. 1711–1717, Jul. 2010, doi: 10.3873/j.issn.1000-1328.2010.07.003.
[16] Y. Wang, S. Xu, and M. Zhu, "Stability of relative equilibria of the full spacecraft dynamics around an asteroid with orbit–attitude coupling," *Adv. Space Res.*, vol. 53, no. 7, pp. 1092–1107, Apr. 2014, doi: 10.1016/j.asr.2013.12.040.
[17] W. H. Clohessy and R. S. Wiltshire, "Terminal guidance system for satellite rendezvous," *J. Aerosp. Sci.*, vol. 27, no. 9, p. 653, 1960, doi: 10.2514/8.8704.
[18] J. Tschauner, "Elliptic orbit rendezvous," *Amer. Inst. Aeronaut. Astronaut.*, vol. 5, no. 6, pp. 1110–1113, Jun. 1967, doi: 10.2514/3.4145.
[19] Z.-P. Xu, X.-Q. Chen, Y.-Y. Huang, Y.-Z. Bai, and W. Yao, "Nonlinear suboptimal tracking control of spacecraft approaching a tumbling target," *Chin. Phys. B*, vol. 27, no. 9, Sep. 2018, Art. no. 090501, doi: 10.1088/1674-1056/27/9/090501.
[20] M. Xin and H. Pan, "Nonlinear optimal control of spacecraft approaching a tumbling target," *Aerosp. Sci. Technol.*, vol. 15, no. 2, pp. 79–89, Mar. 2011, doi: 10.1016/j.ast.2010.05.009.
[21] X. B. Chi, Q. Xu, and Z. Q. Li, "Autonomous rendezvous for a noncooperative space target based on convex optimization guidance," *J. Astronaut.*, vol. 39, no. 11, pp. 68–77, Nov. 2018, doi: 10.3873/j.issn.1000-1328.2018.11.007.
[22] L. Sun, "Passivity-based adaptive finite-time trajectory tracking control for spacecraft proximity operations," *J. Spacecraft Rockets*, vol. 53, no. 1, pp. 46–56, Jan. 2016, doi: 10.2514/1.A33288.
[23] L. Yuan, G. F. Ma, J. W. Dong, C. J. Li, and B. Y. Jiang, "Fixed time terminal sliding mode control for close-range rendezvous," *J. Astronaut.*, vol. 39, no. 2, pp. 195–205, Feb. 2018, doi: 10.3873/j.issn.1000-1328.2018.02.010.
[24] Y. W. Zhu and L. P. Yang, "Mission trajectory design and control for spacecraft proximity relative motion," *J. Astronaut.*, vol. 30, no. 5, pp. 1834–1841, Sep. 2009, doi: 10.3873/j.issn.1000-1328.2009.05.015.
[25] Y. W. Zhu and L. P. Yang, "6-DOF sliding mode control for fast spacecraft circumnavigation mission," *J. Astronaut.*, vol. 30, no. 4, pp. 1482–1488, Jul. 2009, doi: 10.3873/j.issn.1000-1328.2009.00.029.
[26] X. L. Li, "Guidance method of fast fly-around relative to target spacecraft," M.S. thesis, Dep. Control Sci. Eng., Harbin Univ. Sci. Technol., Harbin, China, 2004.
[27] S. Matsumoto, S. Dubowsky, S. Jacobsen, and Y. Ohkami, "Fly-by approach and guidance for uncontrolled rotating satellite capture," in *Proc. AIAA Guid., Navigat., Control Conf. Exhib.*, Austin, TX, USA, Aug. 2003.
[28] J. Liu, H. Li, Y. Luo, and J. Zhang, "Robust adaptive relative position and attitude integrated control for approaching uncontrolled tumbling spacecraft," *Proc. Inst. Mech. Eng., G, J. Aerosp. Eng.*, vol. 234, no. 2, pp. 361–374, Feb. 2020, doi: 10.1177/0954410019866282.
[29] L. J. Liu and H. Y. Li, "Adaptive sliding mode control based on neural network for approaching to an uncontrolled tumbling satellite," *J. Astronaut.*, vol. 40, no. 6, pp. 684–693, Jun. 2019, doi: 10.3873/j.issn.1000-1328.2019.06.009.
[30] K. T. Alfriend, H. Schaub, and D. W. Gim, "Gravitational perturbations, nonlinearity and circular orbit assumption effects on formation flying control strategies," presented at the 23rd Annu. AAS Rocky Mountain Guid. Control Conf., Breckenridge, CO, USA, Feb. 2000.
[31] D.-W. Gim and K. T. Alfriend, "State transition matrix of relative motion for the perturbed noncircular reference orbit," *J. Guid., Control, Dyn.*, vol. 26, no. 6, pp. 956–971, Nov. 2003, doi: 10.2514/2.6924.

[32] T. Carter and M. Humi, "Clohessy-Wiltshire equations modified to include quadratic drag," *J. Guid., Control, Dyn.*, vol. 25, no. 6, pp. 1058–1063, Nov. 2002, doi: 10.2514/2.5010.

[33] M. Humi and T. Carter, "Rendezvous equations in a central-force field with linear drag," *J. Guid., Control, Dyn.*, vol. 25, no. 1, pp. 74–79, Jan. 2002, doi: 10.2514/2.4851.

[34] P. Gurfil, "Generalized solutions for relative spacecraft orbits under arbitrary perturbations," *Acta Astronautica*, vol. 60, no. 2, pp. 61–78, Jan. 2007, doi: 10.1016/j.actaastro.2006.07.013.

[35] Y. Huang and Y. Jia, "Robust adaptive fixed-time tracking control of 6-DOF spacecraft fly-around mission for noncooperative target," *Int. J. Robust Nonlinear Control*, vol. 28, no. 6, pp. 2598–2618, Apr. 2018, doi: 10.1002/rnc.4038.

[36] D. W. Gao, J. J. Luo, W. H. Ma, Z. Y. Kang, and X. G. Chen, "Nonlinear optimal control of spacecraft approaching and tracking a non-cooperative maneuvering object," *J. Astronaut.*, vol. 34, no. 6, pp. 773–781, Jun. 2013, doi: 1000-1328.2013.06.005.

[37] Y. Huang and Y. M. Jia, "Robust relative position and attitude control for non-cooperative fly-around mission," *Control Theory Appl.*, vol. 35, no. 10, pp. 1405–1414, Oct. 2018, doi: 10.7641/CTA.2018.80038.

[38] K. Zhang, N. Qin, and Y. Sun, "Adaptive spacecraft relative position tracking control for non-cooperative target with thrust saturation," presented at the 14th IEEE Conf. Ind. Electron. Appl. (ICIEA), Xi'an, China, Jun. 2019.

[39] D. W. Gao, J. J. Luo, and W. H. Ma, "Approaching and tracking a maneuvering non-cooperative object using Lyapunov approach," *J. Northwestern Polytechnical Univ.*, vol. 31, no. 4, pp. 577–583, Aug. 2013.

[40] H. W. Lan and Y. Jiang, "Study on flying-around guidance law for tracking space target," *Syst. Eng. Electron.*, vol. 30, no. 9, pp. 1735–1739, Sep. 2008.

[41] J. Liu and H. Li, "Artificial potential function safety and obstacle avoidance guidance for autonomous rendezvous and docking with noncooperative target," *Math. Problems Eng.*, vol. 2019, pp. 1–17, Aug. 2019, doi: 10.1155/2019/3451864.

[42] Y.-C. Chiou and C.-Y. Kuo, "Geometric approach to three-dimensional missile guidance problem," *J. Guid., Control, Dyn.*, vol. 21, no. 2, pp. 335–341, Mar. 1998, doi: 10.2514/2.4240.

[43] Y. Meng and Q. Chen, "A new geometric guidance approach to spacecraft near-distance rendezvous problem," *Acta Astronautica*, vol. 129, Sep. 2016, pp. 374–383, doi: 10.1016/j.actaastro.2016.09.032.

[44] K. Li, W. Su, and L. Chen, "Performance analysis of three-dimensional differential geometric guidance law against low-speed maneuvering targets," *Astrodynamics*, vol. 2, no. 3, pp. 233–247, Sep. 2018, doi: 10.1007/s42064-018-0023-z.

[45] K. B. Li and L. Chen, "Comment on 'Partial integrated missile guidance and control with finite time convergence,'" *J. Guid., Control Dyn.*, vol. 39, no. 3, pp. 733–734, Mar. 2016, doi: 10.2514/1.G001448.

[46] W. L. Wang, X. M. Song, and L. Wang, "A modeling method for proximity control to a tumbling target," *J. Astronaut.*, vol. 41, no. 2, pp. 215–223, Feb. 2020, doi: 10.3873/j.issn.1000-1328.2020.02.011.

[47] W. Wang, L. Chen, Y. Lei, and Y. Liang, "Cooperative guidance and control for rendezvous with uncooperative target based on augment proportional navigation," presented at the 35th Chin. Control Conf. (CCC), Chengdu, China, Jul. 2016.

[48] Y. H. Liu, "Research on guidance and control strategy of close-range relative motion against space tumbling target," M.S. thesis, Dep. Aerospace Sci. Technol., Nat. Univ. Defense Technol., Changsha, China, 2018.

[49] J. H. Liu, H. Y. Li, L. Y. Yang, and L. Lu, "Control strategy of forced flying-around uncontrolled rotating targets," *Syst. Eng. Electron.*, vol. 40, no. 10, pp. 2310–2319, Oct. 2019, doi: 10.3969/j.issn.1001-506X.2019.10.21.

[50] J. H. Liu and H. Y. Li, "Augmented proportional navigation control for approach to uncontrolled tumbling satellite," *Syst. Eng. Electron.*, vol. 40, no. 10, pp. 2311–2316, Oct. 2018, doi: 10.3969/j.issn.1001-506X.2018.10.23.

[51] Y. Wang, G. Zhang, Z. Shi, Q. Wang, J. Su, and H. Qiao, "Finite-time speed control of marine diesel engine based on ADRC," *Math. Problems Eng.*, vol. 2020, pp. 1–8, Feb. 2020, doi: 10.1155/2020/2709460.

[52] D. Cai, H. Zou, J. Wang, Y. Huang, and D. Shi, "Event-triggered attitude tracking for rigid spacecraft," *Sci. China Inf. Sci.*, vol. 62, no. 12, pp. 178–193, Dec. 2019, doi: 10.1007/s11432-018-9844-3.

[53] H. Y. Jin, J. C. Song, W. Y. Lan, and Z. Q. Gao, "On the characteristics of ADRC: A PID interpretation," *Sci. China Inf. Sci.*, vol. 6, no. 10, pp. 1–3, Oct. 2020, doi: 10.1007/s11432-018-9647-6.

[54] Z. Wu, Z. Gao, D. Li, Y. Chen, and Y. Liu, "On transitioning from PID to ADRC in thermal power plants," *Control Theory Technol.*, vol. 19, no. 1, pp. 3–18, Mar. 2021, doi: 10.1007/s11768-021-00032-4.

[55] R. Patelski and P. Dutkiewicz, "On the stability of ADRC for manipulators with modelling uncertainties," *ISA Trans.*, vol. 102, pp. 295–303, Jul. 2020, doi: 10.1016/j.isatra.2020.02.027.

[56] Z. Gao and Y. Huang, "A special issue on active disturbance rejection control (ADRC)," *Control Theory Technol.*, vol. 19, no. 1, pp. 1–2, Apr. 2021, doi: 10.1007/s11768-021-00040-4.

[57] X. Yin, J. She, M. Wu, D. Sato, and K. Ohnishi, "Disturbance rejection using SMC-based-equivalent-input-disturbance approach," *Appl. Math. Comput.*, vol. 418, Apr. 2022, Art. no. 126839, doi: 10.1016/j.amc.2021.126839.

[58] K. Adamiak, "Chattering-free reference sliding variable-based SMC," *Math. Problems Eng.*, vol. 2020, pp. 1–16, Sep. 2020, doi: 10.1155/2020/3454090.

[59] L. Ibarra, A. Rosales, P. Ponce, and A. Molina, "Adaptive SMC based on the dynamic containment of the sliding variable," *J. Franklin Inst.*, vol. 358, no. 2, pp. 1422–1447, Jan. 2021, doi: 10.1016/j.jfranklin.2020.12.005.

[60] W. Qi, G. Zong, and H. R. Karimi, "SMC for nonlinear stochastic switching systems with quantization," *IEEE Trans. Circuits Syst. II, Exp. Briefs*, vol. 68, no. 6, pp. 2032–2036, Jun. 2021, doi: 10.1109/TCSII.2020.3047785.

[61] W. Qi, C. Lv, J. H. Park, G. Zong, J. Cheng, and K. Shi, "SMC for semi-Markov jump cyber-physical systems subject to randomly occurring deception attacks," *IEEE Trans. Circuits Syst. II, Exp. Briefs*, vol. 69, no. 1, pp. 159–163, Jan. 2022, doi: 10.1109/TCSII.2021.3076132.

[62] M. Zhang and X. Jing, "Model-free saturated PD-SMC method for 4-DOF tower crane systems," *IEEE Trans. Ind. Electron.*, vol. 69, no. 10, pp. 10270–10280, Oct. 2022.

[63] F. Tieshan, Z. Zhiyao, G. Feng, and L. Baoyu, "Application of adaptive fuzzy ADRC for hypersonic flight vehicle," presented at the 33rd Chin. Control Decis. Conf. (CCDC), Kunming, China, May 2021.

[64] J. J. Liu, M. W. Sun, Z. Q. Chen, and Q. L. Sun, "High AOA decoupling control for aircraft based on ADRC," *J. Syst. Eng. Electron.*, vol. 31, no. 2, pp. 393–402, Apr. 2020, doi: 10.23.919/JSEE.2020.000016.

[65] J. Q. Han, *Active Disturbance Rejection Control Technique*. Beijing, China: National Defense Industry Press, 2013, pp. 69–70.

[66] W. Hu, S. Zhang, W. Xu, J. Yang, and H. Hou, "Based on ADRC strategy for tracking trajectory of undamped plants," *J. Phys., Conf.*, vol. 1906, no. 1, May 2021, Art. no. 012045, doi: 10.1088/1742-6596/1906/1/012045.

[67] J. Hu, Y. Ge, X. Zhou, S. Liu, and J. Wu, "Research on the course control of USV based on improved ADRC," *Syst. Sci. Control Eng.*, vol. 9, no. 1, pp. 44–51, Jan. 2021, doi: 10.1080/21642583.2020.1865216.

[68] L. Li, Y. Ren, X. C. Chen, and Z. Y., "Design of MSCSG control system based on ADRC and RBF neural network," *J. Beijing Univ. Aeronaut. Astronaut.*, vol. 46, no. 10, pp. 1966–1972, Oct. 2020, doi: 10.13700/j.bh.1001-5965.2019.0536.

[69] D. Wu, T. Zhao, and K. Chen, "Research and industrial applications of active disturbance rejection control to fast tool servos," *Control Theory Appl.*, vol. 30, no. 12, pp. 1534–1542, Dec. 2013, doi: 10.7641/CTA.2013.31060.

[70] R. Dong, H. Zhu, and S. Z. Sheng, "Composite controller design of helicopter attitude based on ADRC and SMC," *Electron. Opt. Control*, vol. 27, no. 11, pp. 86–90, Nov. 2020, doi: 10.3969/j.issn.1671-637X.2020.11.017.

[71] W. Hui, Q. Xiaohui, and L. Jie, "Stability analysis of linear/nonlinear switching active disturbance rejection control based MIMO continuous systems," *J. Syst. Eng. Electron.*, vol. 32, no. 4, pp. 956–970, Aug. 2021, doi: 10.23919/JSEE.2021.000082.

[72] J. Li, Y. Xia, X. Qi, and Z. Gao, "On the necessity, scheme, and basis of the linear–nonlinear switching in active disturbance rejection control," *IEEE Trans. Ind. Electron.*, vol. 64, no. 2, pp. 1425–1435, Feb. 2017, doi: 10.1109/TIE.2016.2611573.

[73] A.-M. Zhou, K. D. Kumar, Z.-G. Hou, and X. Liu, "Finite-time attitude tracking control for spacecraft using terminal sliding mode and Chebyshev neural network," *IEEE Trans. Syst., Man, Cybern. B, Cybern.*, vol. 41, no. 4, pp. 950–963, Aug. 2011, doi: 10.1109/TSMCB.2010.2101592.

[74] G. H. Hardy, J. E. Littlewood, and G. Polya, "Inequalities," *Math. Gazette*, vol. 72, no. 462, p. 333, Dec. 1988, doi: 10.1017/S0025557200143451.

[75] S. P. Bhat and D. S. Bernstein, "Continuous finite-time stabilization of the translational and rotational double integrators," *IEEE Trans. Autom. Control*, vol. 43, no. 5, pp. 678–682, May 1998, doi: 10.1109/9.668834.
[76] W. Zhang, *Quantitative Process Control Theory*. Boca Raton, CA, USA: CRC Press, 2011, p. 22.

SHUANG LIANG was born in 1989. She received the B.Eng. and M.Eng. degrees from Dalian Maritime University, Dalian, China, in 2011 and 2016, respectively. She is currently pursuing the Ph.D. degree with Space Engineering University, Beijing, China. Her research interests include spacecraft orbit dynamics, guidance and control, and space mission analysis.

YASHENG ZHANG was born in 1974. She received the B.Eng. and M.Eng. degrees from the National University of Defense Technology (NUDT), China, in 1996 and 1999, respectively, and the Ph.D. degree from Space Engineering University, Beijing, China, in 2006.

She is currently a Professor with Space Engineering University. Her research interests include spacecraft orbit dynamics, constellation design, guidance and control, and space mission analysis. She received the Young Science and Technology Award of China, the National Science and Technology Progress Award, and the Space Fund Award of China.

WEILIN WANG was born in 1988. He received the B.Eng., M.Eng., and Ph.D. degrees from the National University of Defense Technology (NUDT), China, in 2010, 2013, and 2017, respectively.

He is currently a Lecturer. He has published more than 20 articles. His research interests include spacecraft orbit dynamics, guidance and control, and space mission analysis.

LU JIA was born in 1994. She received the B.Eng. degree from the PLA University of Science and Technology, Nanjing, China, in 2016. She is currently pursuing the Ph.D. degree with Space Engineering University, Beijing, China. Her research interests include spacecraft orbit dynamics, constellation design, and space mission analysis.